

RESEARCH ARTICLE

The Carboxy Terminus of the Ligand Peptide Determines the Stability of the MHC Class I Molecule H-2K^b: A Combined Molecular Dynamics and Experimental Study

Esam Tolba Abualrous^{1,2}, Sunil Kumar Saini¹, Venkat Raman Ramnarayan¹, Florin Tudor Ilca¹, Martin Zacharias³, Sebastian Springer^{1*}

1 Department of Chemistry and Life Sciences, Jacobs University Bremen, Campus Ring 1, 28759 Bremen, Germany, **2** Department of Physics, Faculty of Science, Ain Shams University, Cairo, Egypt, **3** Physik-Department T38, Technische Universität München, James-Franck-Strasse 1, 85748 Garching, Germany

* sebastian.springer@queens.oxon.org



CrossMark
click for updates

OPEN ACCESS

Citation: Abualrous ET, Saini SK, Ramnarayan VR, Ilca FT, Zacharias M, Springer S (2015) The Carboxy Terminus of the Ligand Peptide Determines the Stability of the MHC Class I Molecule H-2K^b: A Combined Molecular Dynamics and Experimental Study. PLoS ONE 10(8): e0135421. doi:10.1371/journal.pone.0135421

Editor: Scheherazade Sadegh-Nasseri, Johns Hopkins University, UNITED STATES

Received: February 28, 2015

Accepted: July 21, 2015

Published: August 13, 2015

Copyright: © 2015 Abualrous et al. This is an open access article distributed under the terms of the [Creative Commons Attribution License](https://creativecommons.org/licenses/by/4.0/), which permits unrestricted use, distribution, and reproduction in any medium, provided the original author and source are credited.

Data Availability Statement: All relevant data are within the paper and its Supporting Information files.

Funding: This work was supported by Jacobs University and by the DAAD (German Academic Exchange Service) to ETA.

Competing Interests: The authors have declared that no competing interests exist.

Abstract

Major histocompatibility complex (MHC) class I molecules (proteins) bind peptides of eight to ten amino acids to present them at the cell surface to cytotoxic T cells. The class I binding groove binds the peptide via hydrogen bonds with the peptide termini and via diverse interactions with the anchor residue side chains of the peptide. To elucidate which of these interactions is most important for the thermodynamic and kinetic stability of the peptide-bound state, we have combined molecular dynamics simulations and experimental approaches in an investigation of the conformational dynamics and binding parameters of a murine class I molecule (H-2K^b) with optimal and truncated natural peptide epitopes. We show that the F pocket region dominates the conformational and thermodynamic properties of the binding groove, and that therefore the binding of the C terminus of the peptide to the F pocket region plays a crucial role in bringing about the peptide-bound state of MHC class I.

Introduction

Major histocompatibility complex (MHC) class I molecules are transmembrane receptor proteins that transport intracellular peptides to the cell surface such that cytotoxic T cells can recognize epitopes of viral or tumor origin. The luminal part of an MHC class I heavy chain associates with the light chain beta-2 microglobulin (β_2m) and then binds peptides in the endoplasmic reticulum (ER, [Fig 1A](#)). The stable ternary complex of heavy chain, β_2m , and peptide then travels to the cell surface [[1](#)].

The peptide binding groove, formed by the α_1/α_2 superdomain, consists of an eight-stranded beta sheet platform topped by two alpha helices ([Fig 1B](#)) [[2,3](#)]. The groove is closed at both ends and usually accommodates a peptide of eight to ten amino acids only [[4–6](#)] that extends distinct side chains (called anchor residues) into defined pockets at the bottom of the

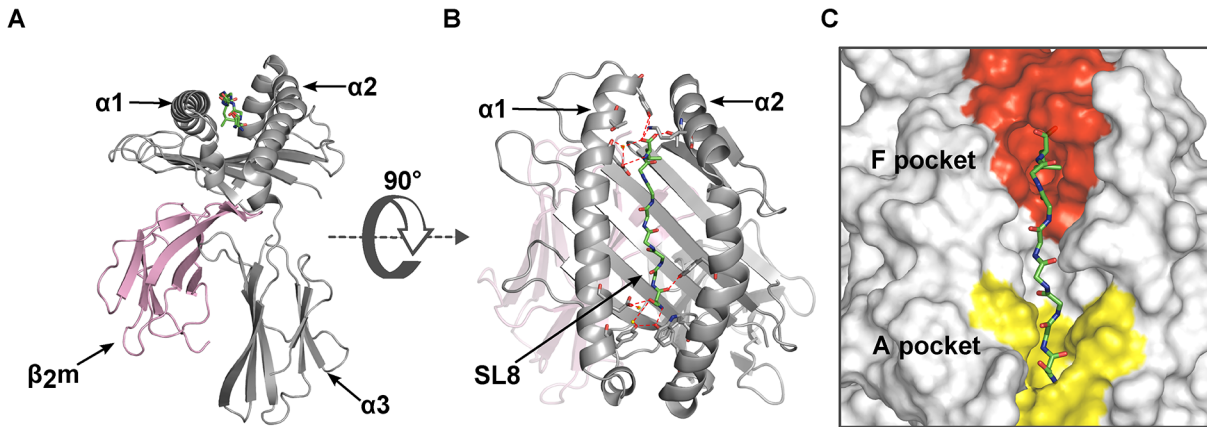


Fig 1. Crystal structure of the luminal domain of H-2K^p. (A) Cartoon representation of class I heavy chain (gray) and the light chain β_{2m} (pink). (B) Top view of the H-2K^p binding groove bound to an octamer antigenic peptide, SIINFEKL, represented as sticks of the peptide backbone (green carbon, red oxygen, and blue nitrogen). The hydrogen bonds between the peptide C and N termini and the binding groove are shown as red dashes. (C) The molecular surface of the F pocket (red) and the A pocket (yellow) of the H-2K^p binding groove (gray).

doi:10.1371/journal.pone.0135421.g001

groove. The peptide amino (N) and carboxy (C) termini form networks of hydrogen bonds in the regions around the A and F pockets at the ends of the groove (Fig 1C) in all class I/peptide complexes whose structure has been determined [7–9]. For stable binding to class I, optimal anchor residues are not strictly required [10–13].

In the cell, optimally loaded class I molecules are formed by selecting high-affinity peptides (*i.e.*, peptides with a low dissociation rate) from the large pool of cellular peptides. This is central to the function of a class I molecule, since the complex must persist at the cell surface for hours to allow interactions with T cells [14]. The chaperone protein tapasin supports the selection of peptides in the ER that fulfill the specific length and sequence requirements for binding. There is no crystal structure of a tapasin-class I complex, but there is experimental and theoretical evidence that tapasin binds close to the F pocket [15–18].

To understand and eventually predict peptide selection in the cell, we will need to properly understand the binding energy contributions of each individual peptide-class I interaction, especially of the peptide termini. Empty class I molecules are suggested by several studies to be very flexible and energetically unstable [19–22]. Several lines of evidence suggest that in optimally loaded class I molecules, the restraint of the movements of the class I molecule by the peptide is a central feature of the peptide-bound state. To understand the energy contribution of the peptide interactions in stabilizing class I, Marlene Bouvier and Don Wiley first used circular dichroism to measure the midpoint of the thermal denaturation curve (T_m , 'melting temperature') of HLA-A*02:01 folded *in vitro* in the presence of different truncated and modified peptides. Removal of the N-terminal amino group reduced the T_m by 21 K, whereas removal of the C-terminal carboxylate reduced it by 23 K. Based on this observation, they suggested that the interactions at C or N terminus peptide make the highest energetic contribution to the stability of the complex [20].

With the help of molecular dynamics (MD) simulations, we and others then showed that in murine and human class I molecules, the sections of the α_1 and α_2 helices around the F pocket that bind the peptide C terminus are conformationally flexible on a nanosecond time scale when no peptide is bound, whereas the A pocket region, which accommodates the N terminus of the peptide, is much more rigid and does not differ much in flexibility between the peptide-bound and peptide-empty states [23–26].

Experimental results support the role of the peptide C terminus in the conformational stabilization of class I [12]. A crystal structure of an empty class I molecule has not yet been obtained, but the B values of class I/peptide crystal structures show higher flexibility for the F pocket region than for the A pocket region [27–30]. The position of the F pocket region residues, especially the N terminus of the α_2 helix, differs between crystal structures of the same class I allotype, suggesting a certain amount of adaptability of the F pocket region [23]. The crystal structure of H-2D^b with the pentapeptide NYPAL, which occupies the F but not the A pocket, is almost identical to that of D^b with full-length peptide [31]. With thermal denaturation experiments, we have shown that dipeptides that resemble the C termini of high-affinity peptides, and that presumably bind into the F pocket, help class I molecules to fold and protect them from denaturation [32].

In apparent contrast to these data, others have demonstrated that a 3_{10} -helical fragment close to the A pocket changes conformation upon peptide binding to H-2L^d, and they have proposed that this is the main conformational change in class I upon peptide binding [33]. Likewise, in our previous work, connecting the α_1 and α_2 helices by a disulfide bond close to the F pocket (which greatly restrains the mobility of this region in MD simulations) still allows normal chaperone interaction, peptide binding, and antigen presentation [34], suggesting that stabilization of the F pocket region by the peptide may not be essential for peptide binding to class I.

To precisely understand the contribution of individual functional groups of the peptide, especially the termini, to peptide binding, we have now combined MD simulations with biochemical and cellular approaches and studied the thermodynamic and conformational details of the binding of truncated and modified peptides. We find that the binding of the peptide C terminus to the F pocket is central to the conformational and thermal stability of the H-2K^b/peptide complex. F pocket occupancy slows peptide dissociation and retains class I on the cell surface. Our work expands the molecular understanding of the details of the class I-peptide binding process, which will advance the ability to design vaccines for given peptides, and the development of small molecules that influence class I antigen presentation.

Materials and Methods

Molecular dynamics (MD) simulations

The crystal structures of H-2K^b in complex with the high-affinity peptides SIINFEKL and FAPGNYPAL (PDB ID code 1VAC [11] and 1KPV, respectively) served as the starting structure for the MD simulations, which were performed as in [35]. The detailed protocols are found in the supporting information.

Thermal denaturation by tryptophan fluorescence (TDTF) measurements

TDTF measurements and T_m determination were performed exactly as described previously [36]. The detailed protocols are found in the supporting information.

Half-maximal inhibitory concentration (IC₅₀) measurements

Steady state measurements were performed with peptide-free folding reactions of K^b/β₂m. Following ultracentrifugation, different concentrations of full-length, truncated, or modified peptides were added for 5 min, and the competitive binding of 100 nM of the high affinity peptide SIINFEK-TAMRA_L, labeled with carboxytetramethylrhodamine (TAMRA) on the lysine side chain, was measured by anisotropy in the Cary fluorimeter with automated polarizers.

Brefeldin A (BFA) decay assay

RMA-S cells [37] were kept overnight at 25°C and at t = 0 treated with 10 µg/ml BFA (Applchem or Alfa Aesar) and with 10 µM peptide and transferred to 37°C for a maximum of 4 hours. At different time points, cells were washed twice with 1x PBS/0.01% NaN₃, and cell surface K^b was measured with the MAb Y3 by flow cytometry.

Results and Discussion

The peptide C terminus restrains the conformational dynamics of H-2K^b

We first investigated the effect of the terminal residues of the peptide on the conformational stability of the murine MHC class I allotype H-2K^b (K^b) in MD simulations. As starting structures, we used published crystal structures of K^b bound to the high-affinity peptides SIINFEKL (K^b/SIINFEKL; sequence in single-letter amino acid code) and FAPGNYPAL (K^b/FAPGNYPAL) to construct models of K^b without peptide (empty: eK^b_{SIINFEKL} and eK^b_{FAPGNYPAL}). We performed MD simulations with these four structures and measured the root mean square deviation (RMSD) for all residues that form the binding groove (res. 1–180). The binding grooves of both K^b/SIINFEKL and K^b/FAPGNYPAL showed narrow RMSD probability distribution peaks (Fig 2). Without peptide, in contrast, RMSD values were higher on average and

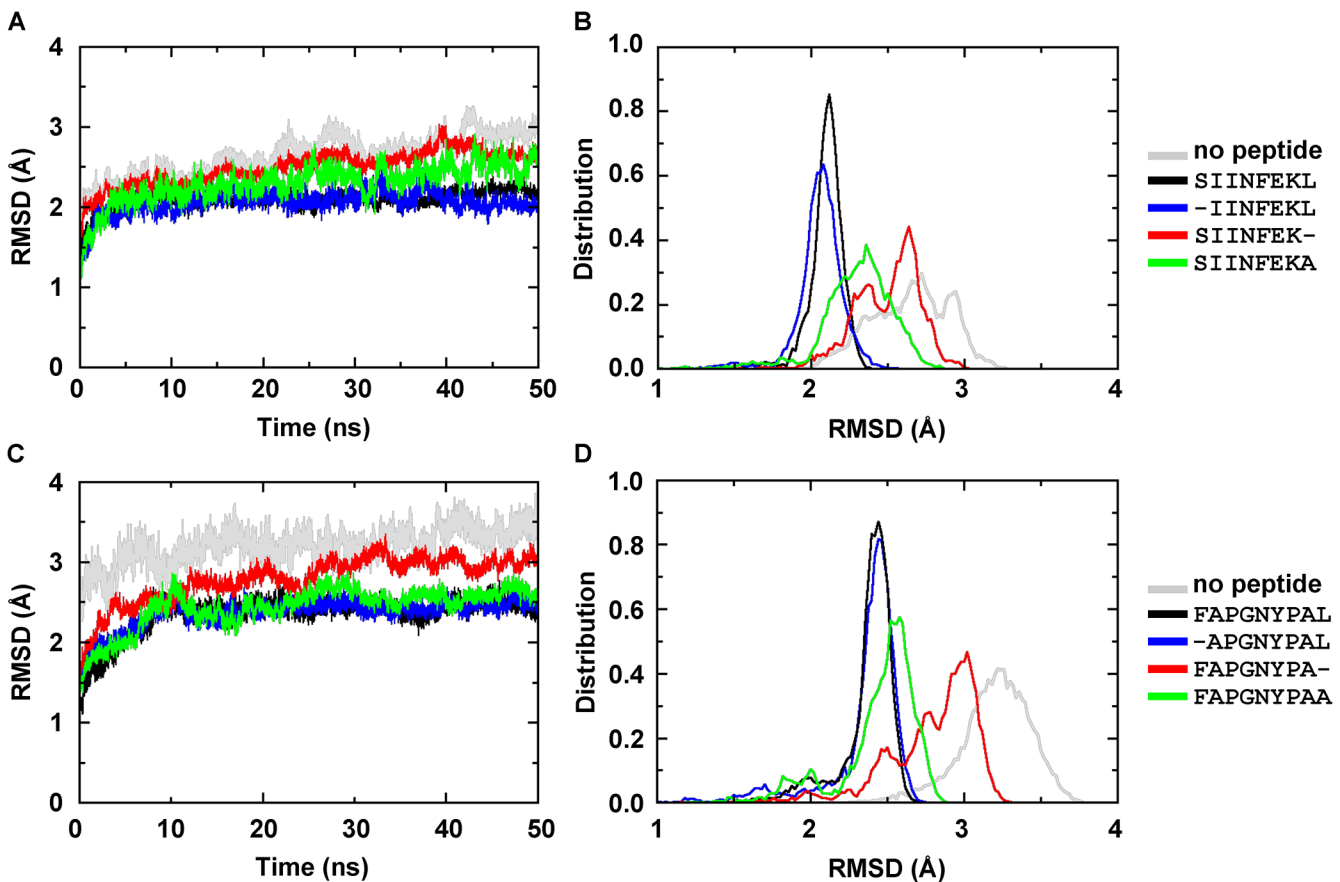


Fig 2. Root mean square deviation (RMSD) of the binding groove of H-2K^b (residues 1–180, gray), bound to the indicated peptides. The values were calculated from frames of two independent MD simulations. (A) RMSD time course for trajectories of the complexes derived from the K^b/SIINFEKL crystal structure. (B) RMSD probability distribution of all trajectories for each molecule. (C) RMSD time course for the trajectories of the complexes derived from the K^b/FAPGNYPAL crystal structure. (D) RMSD probability distribution calculated over the trajectories for each molecule.

doi:10.1371/journal.pone.0135421.g002

more widely distributed, suggesting greater conformational fluctuation. Thus, as reported before [6,12,24,35,38,39], the total lack of peptide conformationally destabilized the binding groove.

To distinguish whether this destabilization was caused by the loss of binding of the peptide N terminus, the peptide C terminus, or both, we next performed and analyzed MD simulations of K^b bound to peptides that were truncated by a single residue at either end. When the C-terminal residue of the peptide (in the following abbreviated as $P\omega$) was truncated (K^b /SIINFEK and K^b /FAPGNYPAA), the RMSD values of the binding groove increased towards those of the empty binding groove. In surprising contrast, truncation of the peptide N terminus (K^b /IINFEKL and K^b /APGNYPAL) did not significantly affect the RMSD (Fig 2B and 2D). This suggests that binding of $P\omega$ is necessary to restrict the conformational motion of K^b .

To differentiate between the stabilizing contributions of the carboxylate group and the $P\omega$ side chain, we simulated K^b complexes with peptides whose $P\omega$ was modified to alanine. The binding grooves of K^b /SIINFEKA and K^b /FAPGNYPAA complexes showed RMSD average values only slightly higher than those with the full-length peptide (with slightly broader peaks; Fig 2B and 2D; green). Impressively, however, when $P\omega$ of SIINFEKL was modified to glycine (SIINFEKG), entirely removing the side chain, we saw a significant increase in the RMSD, suggesting that even the small methyl group in the side chain of a C-terminal alanine helps stabilize the binding groove (S1A and S1B Fig).

When we removed the $P\omega$ carboxylate group of the peptide (replacing the leucine with isopentylamine to give the K^b /SIINFEKL-Cdel complex), we saw similarly strong destabilization (S1A and S1B Fig). Thus, both the $P\omega$ side chain and the carboxylate are important to restrain the flexibility of the binding groove.

The peptide C terminus restrains the mobility of the F pocket region

To see which residues of the class I binding groove are conformationally stabilized by peptide binding, we next measured the root mean square fluctuation (RMSF) of each residue of the binding groove and colored the structure accordingly with a blue to red color spectrum (heat map; Fig 3 and S1C Fig). The binding grooves of the empty molecules were highly flexible, especially in the F pocket region, and the class I residues that bind the $P\omega$ showed the highest flexibility when the binding pocket was empty. Binding of the full-length peptides restrained the flexibility of these residues, but peptides that lacked $P\omega$ had no such restraining effect. For SIINFEKA, SIINFEKG and SIINFEKL-Cdel, the restraint was intermediate. In contrast, the K^b residues surrounding the A pocket always remained at similar levels of flexibility, whether without peptide, with full-length peptides, or with N- or C-terminally truncated peptides. Since the RMSF correlates with the configuration entropy ΔS_{config} (*i.e.*, the entropy related to the position of the atoms rather than their velocity or momentum; [25, 26]), we conclude that in the peptide-empty state, the F pocket residues possess a high ΔS_{config} that is restrained upon peptide binding, whereas the remainder of the binding groove has a similar ΔS_{config} in both empty and peptide-bound structures.

Binding free energy analysis shows a cooperative effect of the carboxylate group and the side chain

To more precisely quantify the role of the peptide N and C termini in the conformational stability of the K^b /peptide complex, we calculated the free energy of peptide binding (ΔG) to the binding groove for both sets of MD simulations by combining the molecular mechanics force fields and the continuum solvation model [40–42] in the molecular mechanics Poisson-Boltzmann surface area (MM-PBSA) method (S1 Table). MM-PBSA performs well in measuring

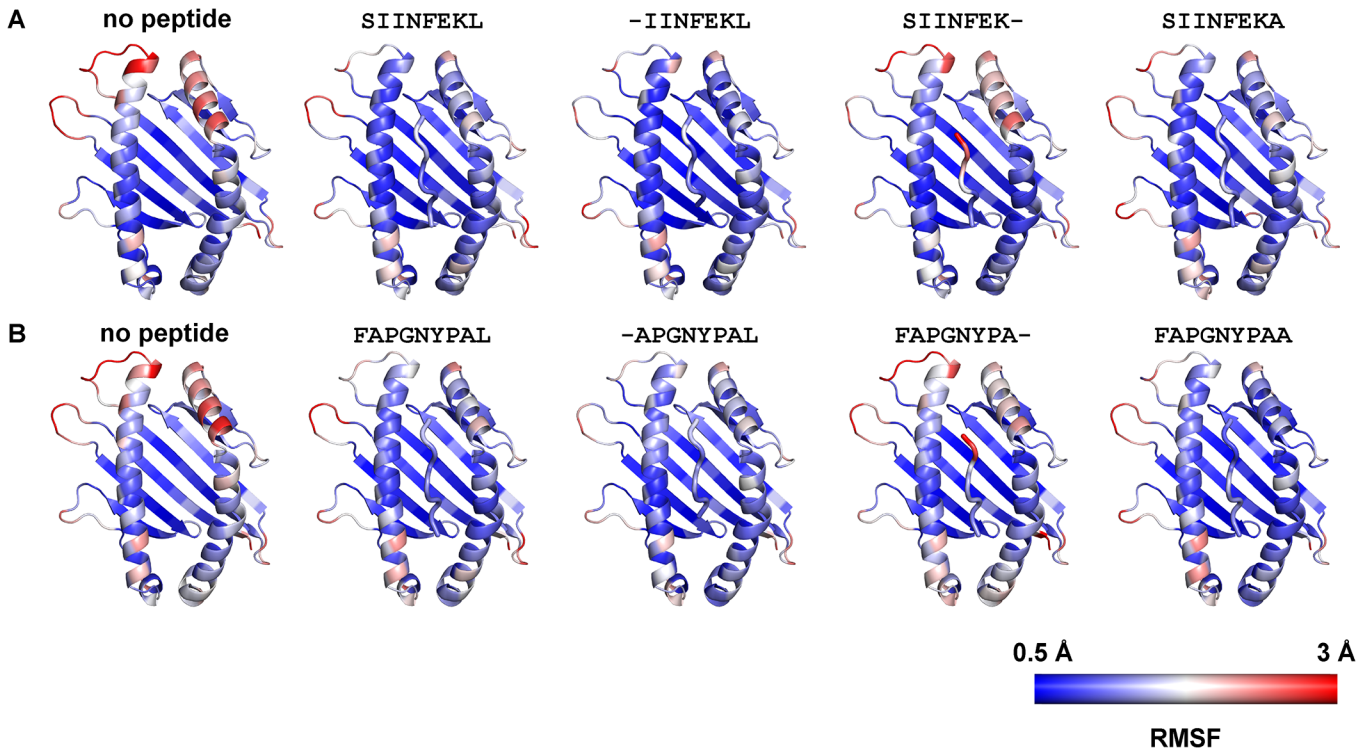


Fig 3. Color-coded view of the configurational flexibility of K^b binding groove and peptide calculated as root mean square fluctuations (RMSF) for each individual residue of the protein from two independent MD simulations of complexes with peptide derived from the (A) K^b /SIINFEKL or (B) K^b /FAPGNYPAL structures and depicted as a color (blue to red) on a cartoon representation of K^b . The empty molecule and the K^b /C-terminally truncated peptide complex show high flexibility of the alpha helices lining the F pocket.

doi:10.1371/journal.pone.0135421.g003

the relative values of receptor-ligand binding free energies [43–47]. It does not include the entropy term, which is very computationally demanding, but in earlier work, inclusion of the entropy term did not necessarily improve the prediction accuracy [46,48].

To rank the peptides based on their binding free energy, we then calculated the change in the binding free energy ($\Delta\Delta G_{MM-PBSA}$, S1 Table) that occurs upon modifying or truncating the peptide. The $P\omega$ truncations showed a much higher $\Delta\Delta G_{MM-PBSA}$ than the N-terminal truncations, suggesting a major contribution of the $P\omega$ to the peptide binding energy. Looking in more details, the change in $\Delta\Delta G_{MM-PBSA}$ was greater when the $P\omega$ carboxylate was removed than for the complexes with alanine- and glycine-modified C termini. This suggests an important contribution of the hydrogen bonds of the $P\omega$ carboxylate to the binding energy.

To test our ranking by experiment, we next used the TDTF (thermal denaturation measured by tryptophan fluorescence) assay to determine the T_m of the K^b /peptide complexes. In this assay, thermal unfolding of the class I molecule is measured by the decrease in fluorescence intensity that occurs when the tryptophan indoles are exposed to the aqueous environment [49,50]. The TDTF analysis was performed on the luminal domain of K^b , which was produced in *E.coli* and folded from inclusion bodies as a complex with human β_2m and with or without peptide [36]. The empty K^b molecule showed the lowest T_m (33°C), and binding of the full-length peptides increased the T_m dramatically (55.7°C for K^b /SIINFEKL and 51.3°C for K^b /FAPGNYPAL; Fig 4A and 4B and S1E Fig; and S2 Table). The complexes with alanine- and glycine-modified $P\omega$, and those where the $P\omega$ carboxylate was removed, still showed some thermodynamic stabilization of K^b . Such stabilization also occurred with N-terminal residue truncations, but with the $P\omega$ truncations K^b /SIINFEK and K^b /FAPGNYP A-, no stabilization of

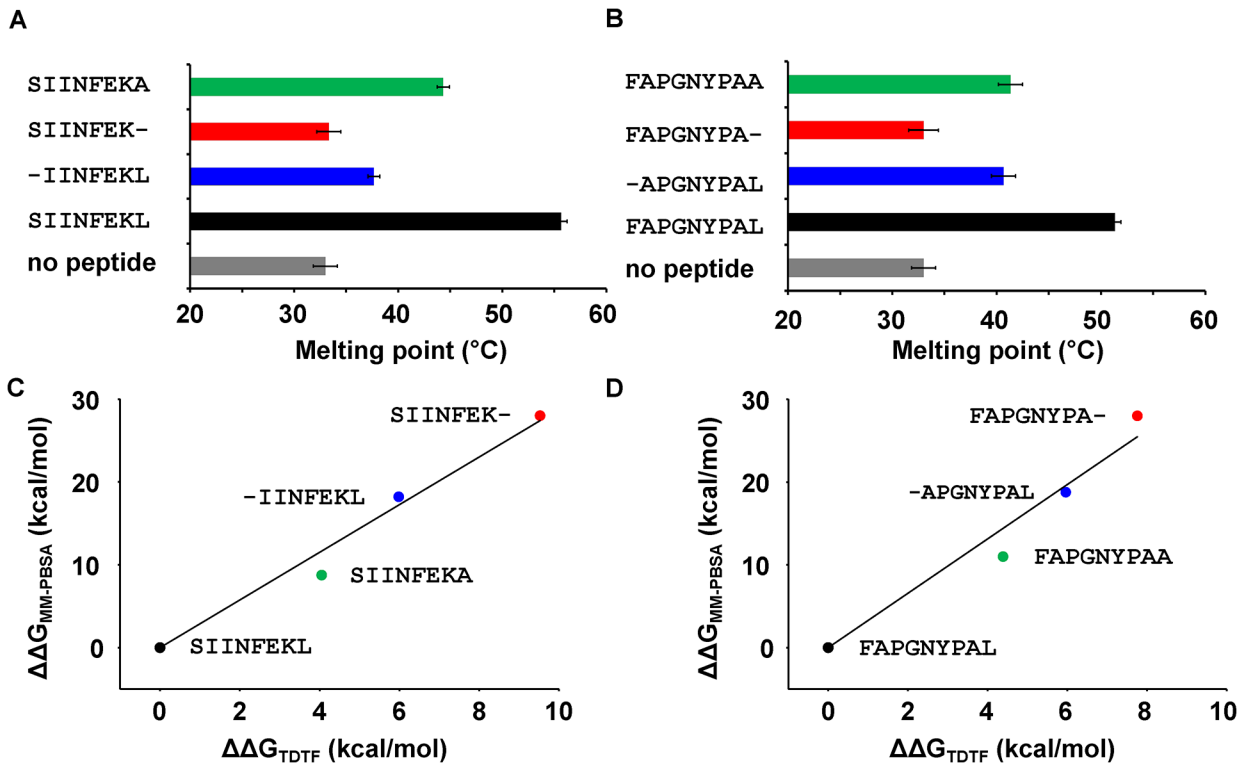


Fig 4. Thermal denaturation measured by tryptophan fluorescence (TDTF) shows the T_m of K^b/β₂m empty or in complex with peptide. (A) K^b/β₂m complexes folded empty or with SIINFEKL-derived peptide as indicated. (B) Analogous experiment, K^b/β₂m complexes with FAPGNYPAL-derived peptides. (C) and (D) correlations between ΔΔG values calculated from TDTF T_m (in A, B) and ΔΔG values from MM/PBSA (S1 Table).

doi:10.1371/journal.pone.0135421.g004

the empty form at all was seen, as we reported before [36]. From the T_m values, we derived the ΔΔG_{TDTF} values using the two-state model of denaturation [50,51]. They correlate very well with the ΔΔG_{MM-PBSA} (correlation coefficients 0.97 and 0.95, Fig 4C and 4D).

Taken together, both theory and experimental data demonstrate in correlation a cooperative effect of the carboxylate group and the side chain at the C terminus of the peptide, which thus contributes much more to the binding energy and conformational stability of the K^b/peptide complex than the N-terminal amino acid.

Both C-terminal side chain and carboxylate are required for high binding affinity of the peptide

Next, we assessed the tendency of each modified peptide to become exchanged for a high-affinity peptide. We followed the hypothesis that greater flexibility of the binding groove in the MD simulations indicates a less perfect fit and thus correlates with lower binding affinity of the bound peptide. This was previously postulated for both class I and class II molecules [25,33,52,53].

To quantify the variation of the binding groove width on a local scale, we divided the binding groove into three regions (region I, which contains the A pocket, region II, in the center of the binding groove, and region III, which contains the F pocket; Fig 5A) and measured their width variation (WV) in the simulations. In all three regions, the WV was greatest when the binding groove was empty, similar to published data [54,55] (Fig 5B and 5C). With the full-length peptide bound, the WV decreased by ca. 0.2 Å² in regions I and II compared to the

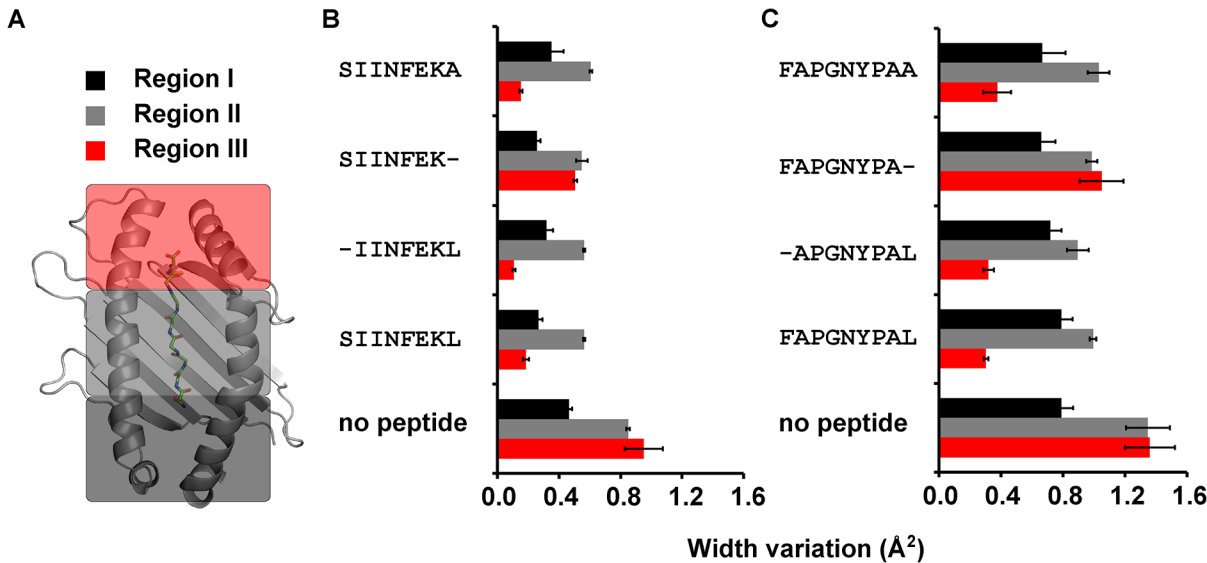


Fig 5. Variation of the binding groove width in MD simulations. (A) Region I (black, A pocket region, residues 50–59 and 165–176), Region II (gray, C pocket region, residues 60–72 and 152–164), and Region III (red, F pocket region, residues 73–84 and 139–150). (B) and (C) Width variance of each region measured as the distance of the centers of masses of the α carbons of respective opposing helical segments for complex derived from the SIINFEKL (B) and FAPGNYPAL (C) crystal structures. Error bars represent standard deviation.

doi:10.1371/journal.pone.0135421.g005

empty molecule, but by a drastic 0.7 to 0.9 Å² in region III. Thus, in agreement with the results shown in Fig 3, the bound peptide had the greatest stabilizing effect on the F pocket region.

The WV of region III for all complexes with truncated and mutated peptides was in the same range as for the full-length peptide complexes (Fig 5B and 5C, and S1E Fig), with the only exception of the P ω truncated peptides SIINFEK and FAPGNYP, which showed large WV, just like the empty K^b molecules. This shows that only the loss of the entire C-terminal amino acid causes a significant conformational fluctuation of the entire F pocket region.

To test by laboratory experiment whether this conformational fluctuation indeed causes a lower complex stability of the P ω truncated peptides, we quantified the affinity of peptides to K^b. K^b was folded empty [36] and then incubated with different concentrations of each peptide variant for five minutes. Then, the index peptide SIINFEK_{TAMRAL} (fluorescently labeled on the lysine side chain) was added as a competitor, and the endpoint of its binding was measured by fluorescence anisotropy [56]. From theory curves fitted to the data, we calculated the half-maximal concentration of inhibition of SIINFEK_{TAMRAL} binding (IC₅₀) for each modified peptide (Fig 6, S1F Fig). We found that the IC₅₀ values of nearly all peptide were similar, but those of the P ω truncated peptides SIINFEK and FAPGNYP were one to two orders of magnitude higher. The experimental data confirm the conclusions from our MD simulations: the loss of the both the P ω carboxylate and the P ω side chain of the peptide destabilize the binding groove and thus facilitate dissociation of the bound peptide and subsequent binding of a new peptide.

Engagement of the C terminus of the peptide retains class I molecules at the cell surface

Once at the cell surface, class I molecules are subject to a quality control—of unknown molecular mechanism—that results in rapid endocytic destruction of those complexes with low-affinity or no peptides [34]. To determine whether the role of the P ω in maintaining a stable class I/peptide complex also applies on the surface of live cells, we tested the stability of our K^b/peptide complexes in a brefeldin A (BFA) decay experiment. Transporter associated with antigen

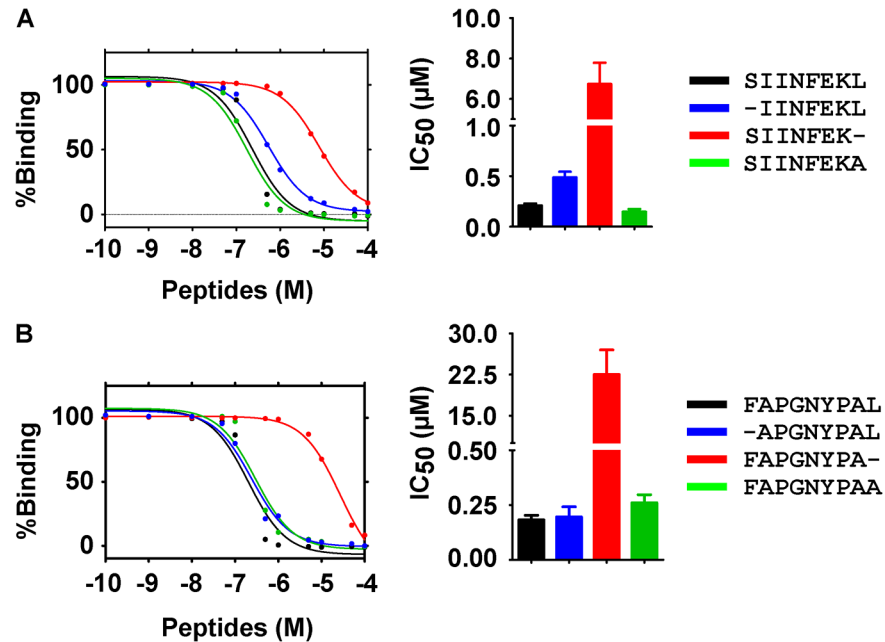


Fig 6. Half-maximal concentration of peptide (IC₅₀) required to inhibit the binding of the high affinity peptide SIINFEK_{TAMRA}L. K^b/β₂m complexes derived from the SIINFEKL (A) or the FAPGNYPAL (B) structures were folded empty and then incubated for 5 minutes with different concentrations of full-length, truncated, or modified peptides. The Pω truncated peptide shows the highest IC₅₀ value. Numerical IC₅₀ values: SIINFEKL, 0.19 μM; IINFEKL, 0.43 μM; SIINFEK, 7.7 μM; SIINFEKA, 0.12 μM; FAPGNYPAL, 0.16 μM; APGNYPAL, 0.15 μM; FAPGNYPAL-, 18.0 μM; FAPGNYPAA, 0.22 μM. Binding curves (left) are of one representative experiment, and the IC₅₀ values (right) are the average of three experiments.

doi:10.1371/journal.pone.0135421.g006

processing (TAP)-deficient RMA-S cells, which cannot load high-affinity peptides onto K^b, were kept overnight at 25°C to accumulate peptide-receptive class I molecules at the cell surface [37,57,58]. We then incubated these cells with each peptide and measured the surface residence time of the K^b/peptide complexes by withdrawing aliquots of cells at different times, fixing, and staining with the antibody Y3 followed by flow cytometry (Fig 7, S11 Fig). As expected, more than 80% of the K^b/SIINFEKL and K^b/FAPGNYPAL complexes remained on the cell surface after four hours, whereas without peptide addition, about 50% of peptide-receptive K^b molecules were endocytosed after only 50 min of incubation. In comparison of the variant peptides, SIINFEK and FAPGNYPAL showed the lowest efficiency in stabilizing K^b on the cell surface, whereas the Pω side chain and carboxylate deletions stabilized K^b to an intermediate extent. Thus, under the conditions of cell surface quality control, binding of the Pω is critically important for retaining class I at the surface.

The free binding energy profile of the peptide C terminus in the F pocket depends on its side chain

Finally, we investigated in more detail the impact of altering the Pω side chain on the free energy profile of the peptide C terminus in the F pocket. We used umbrella sampling (US) simulations to compare the energy barriers along the dissociation pathway of the Pω (Fig 8A and 8B and S3 Fig). We simulated the K^b/peptide complexes at different distance windows between the alpha carbon of the Pω and the bottom of the F pocket. Starting from the experimental crystal structure, the dissociation of the Pω from the F pocket was enforced, and weighted histogram analysis was employed to calculate the free energy profile along the reaction coordinate.

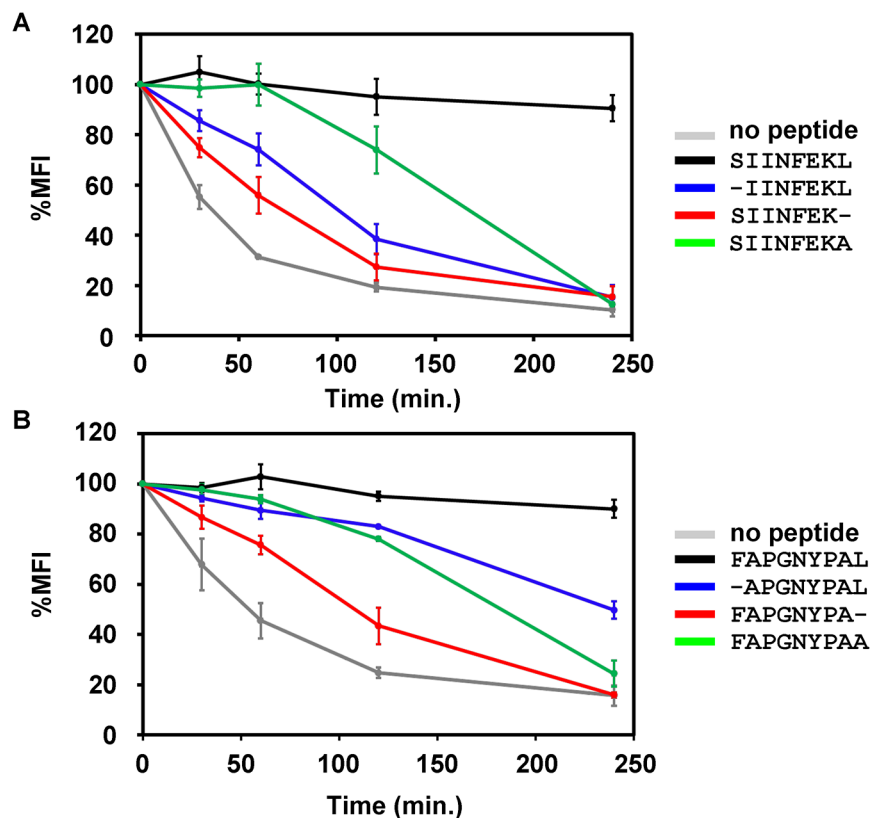


Fig 7. The K^b/C-terminally truncated peptide complex shows the lowest stability on the cell surface in a BFA decay experiment. RMA-S cells were incubated overnight at 25°C, then 10 μM peptide (as indicated) was added to the medium, and cells were transferred to 37°C. H-2K^b surface levels were determined at each time point with MAb Y3 and flow cytometry. Averages ± SEM (n = 3) are normalized to initial mean fluorescence intensity (MFI).

doi:10.1371/journal.pone.0135421.g007

The Pω leucine of the peptides SIINFEKL and IINFEKL had a free energy barrier that was ca. 11 kcal/mol higher than the Pω alanine or glycine (SIINFEKA, SIINFEKG) at a distance of 17 Å from the bottom of the F pocket, whereas the truncation of the Pω carboxylate (SIINFEKL-Cdel) showed ca. 5 kcal/mol at the same distance (Fig 8A, S1G Fig). In a similar manner, the Pω leucine in both FAPGNYPAL and APGNYPAL had a free energy barrier of ca. 8 kcal/mol higher than the Pω alanine (FAPGNYPAA) at a distance 16 Å from the bottom of the F pocket (Fig 8B). These data suggest that the F pocket of K^b requires both a long bulky side chain [59,60] and the Pω carboxylate for tight binding of the C terminus of the peptide.

Discussion and Conclusions

Many attempts have been made to describe the molecular details of peptide binding to class I [7,9,12,55,61]. The interactions that occur between the peptide termini and the residues in the A and F pocket make the major energy contribution to binding [9,12,61,62]. Binding of the peptide N terminus into the A pocket is mainly via a network of hydrogen bonds with a group of conserved tyrosine residues [11]. At the other end of the binding groove, the C terminus of the peptide binds to residues in the F pocket region, also via hydrogen bonds [12]. The orientation of the peptide allows the Pω side chain to be buried deeply within the F pocket (Fig 1B).

Most previous studies of peptide binding to class I only compare optimally loaded class I molecules with empty ones [24,25,53,63]. However, suboptimally loaded class I molecules have

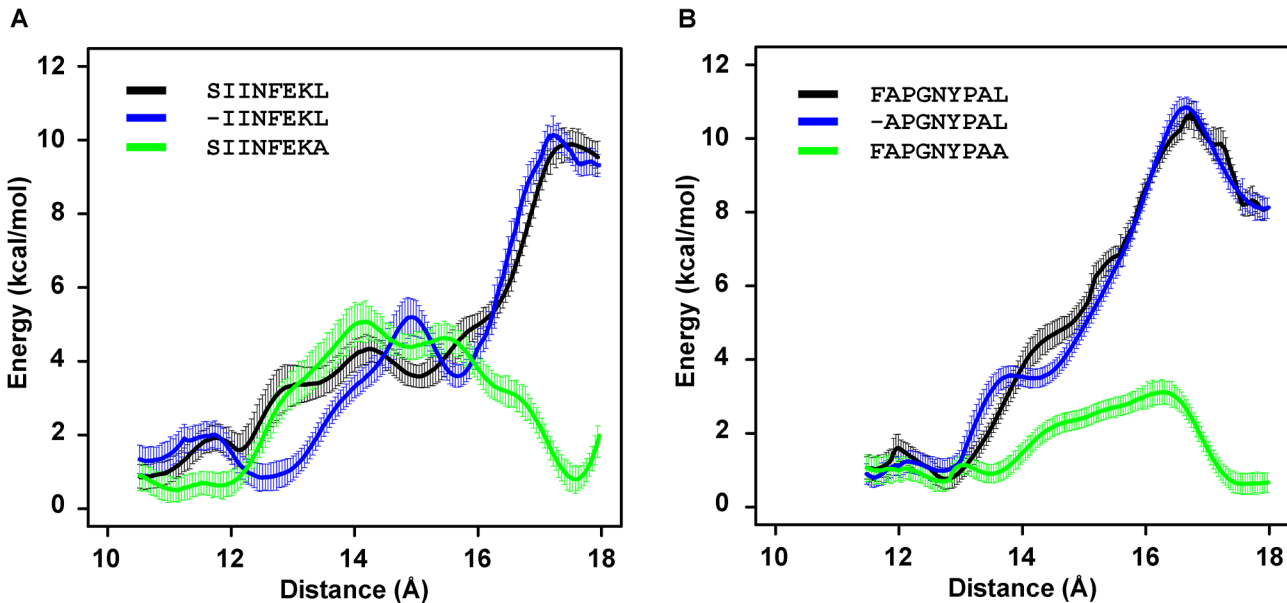


Fig 8. Calculated free energy change (potential of mean force, PMF) obtained from umbrella sampling simulations along the distance between the alpha carbon of the P ω and the bottom of the F pocket. Free energy changes were extracted from simulations of complexes with peptides derived from K^b/SIINFEKL (B) or K^b/FAPGNYPAL (C) structures. The start point and end point reaction coordinates are shown in the supporting material (S3 Fig).

doi:10.1371/journal.pone.0135421.g008

thermodynamic and conformational properties that yield a better understanding of peptide binding [19,31,32]. In this study, we have performed MD simulations of K^b molecules bound to natural full-length peptides and to their suboptimal variants that were truncated or altered at their termini in order to determine the effect of peptide truncations on the dynamics and binding energy of the class I peptide binding groove. Since no crystal structures of empty or suboptimally loaded class I molecules are available (except for D^b/NYPAL, [31], we started all simulations with the crystal structures of the high-affinity peptide complexes K^b/SIINFEKL and K^b/FAPGNYPAL that we modified to obtain the peptide truncations. To minimize the risk that the trajectories might be guided by the starting structure, we used two different starting crystal structures (see the [materials and methods](#)), and we energy-minimized and equilibrated all structures before starting the simulations. Our simulations cannot fully ensure that in the test tube, the short peptides bind in the same register to class I as the full-length peptides, but the closed ends of the class I binding groove and its topology make it likely.

Our MD simulations show a greater conformational stability for optimally loaded complexes compared to empty class I molecules, which confirms the need for the full-length peptide to restrain the conformational motions of K^b binding groove [23–25]. Interestingly, and in contrast to published data for the murine allotype H-2L^d [33], the complexes with truncated peptide N terminus show the same degree of conformational restriction as with full length peptide, whereas truncation of the peptide C terminus results in high flexibility of the F pocket region, similar to that of the empty groove (Figs 2 and 3). Our results are consistent with previous MD simulation studies of human and murine allotypes (H-2D^b, H-2K^b and HLA-B*27:05) [23,24,32,39] and suggest that the binding of the P ω to the flexible F pocket region is required to restrain such flexibility and stabilize the class I binding groove. This major role of the F pocket region in the stability of the K^b/peptide complex is confirmed by the TDTF results (Fig 4A and 4B). We have shown previously that upon heating of a complex of K^b with a suboptimal peptide, the peptide dissociates quickly from the binding groove, and the empty class I denatures [36].

If the complex of K^b with C-terminally truncated peptides is less resistant to heat, it might also show a higher dissociation rate at room temperature. Indeed, the IC_{50} values in Fig 6 strongly point to a major role of the $P\omega$ in maintaining peptide binding to class I, indicating that as long as the F pocket is occupied by the $P\omega$, it is difficult to exchange the bound peptide. This is especially important since peptide dissociation co-determines the peptide exchange and optimization in the cell [64–66]. On the cell surface, truncation of the $P\omega$ increases the endocytosis rate of class I (Fig 7). This is probably because of the drastic decrease in the ΔG of the complex (S1 Table).

Our data suggest a common model where the peptide binding groove of K^b has two dynamic states, peptide-bound and peptide-empty. The biggest difference between these states is visible in the F pocket region. In the peptide-bound state, the helices of the F pocket region are rigid, and their distance is constant. In the peptide-empty state, the helices of the F pocket region are very flexible, and their distance fluctuates. It has been shown experimentally that the helices may partially unfold on a longer time scale [67]. We have found that binding of the $P\omega$ triggers the transition between the peptide-empty and the peptide-bound states and thus determines the peptide-bound conformation of the entire class I molecule.

Our data reveal a synergistic effect of the carboxylate group and the $P\omega$ side chain. Compared to the effect of the removal of the $P\omega$, the truncations of either the carboxylate group or the side chain show an intermediate effect on the conformational and thermal stability of the complex. Thus, we suggest that this role of the $P\omega$ in the F pocket region follows an entropy-enthalpy compensation pathway, as observed previously for the binding between class I and the T cell receptor [68–72]. The binding enthalpy increases via a network of hydrogen bonds with the peptide C terminus, whereas the entropy is restrained by the binding of the $P\omega$ side chain to the bottom of the F pocket.

The prominent role of the F pocket region in our model is consistent with binding of tapasin close to the F pocket region of class I to mediate thermodynamic stabilization of class I as well as peptide exchange and optimization, as suggested previously [15–17,19,21,73,74]. We assume that tapasin helps to structure the F pocket region of a suboptimally loaded class I molecule such that it can bind optimal peptide [39].

Our data support the notion that short peptides and similar small compounds can be used to stabilize class I proteins on the cell surface in a peptide-receptive conformation. This is especially important for efficient T cell activation and improved vaccination. It also opens a window for the modelling of small compounds to bind specifically to the F pocket region and thus enhance or inhibit the binding of the peptide ensemble in a predefined conformation.

In agreement with previous MD studies, which have shown that the dynamics of different domains in class I and other proteins might be coupled [25,75], the findings in this work enable further analysis of the impact of the F pocket region on the global dynamics of other class I domains and the entire protein. Our study also illustrates that MD simulations can be complemented by experimental data to describe the mechanism of ligand-receptor binding and to provide atomic-level details that help in understanding its molecular basis.

Supporting Information

S1 Fig. (A) RMSD time course for trajectories of the complexes derived from the K^b /SIINFEKL crystal structure. (B) RMSD probability distribution of all trajectories for each molecule eK^b /SIINFEKL shows four distinct peaks (approx. 2.3, 2.6, 2.8, and 3.2 Å), whereas K^b /SIINFEKL show narrow peaks at 2.2 Å. K^b /SIINFEKG shows broad peak at 2.8 Å and K^b /SIINFEKL-Cdel shows two peaks at 2.5 and 3 Å. (C) Color-coded view of the configurational flexibility of K^b binding groove and peptide calculated as root mean square

fluctuations (RMSF) for each individual residue of the protein from MD simulations of peptide complexes K^b /SIINFEKG and K^b /SIINFEKL-Cdel. (D) Variation of the binding groove width in MD simulations. A: Region I (black, A pocket region, residues 50–59 and 165–176), Region II (gray, C pocket region, residues 60–72 and 152–164), and Region III (red, F pocket region, residues 73–84 and 139–150). (E) Thermal denaturation measured by tryptophan fluorescence (TDTF) shows the T_m of K^b/β_2m empty or in complex with peptide. (F) Half-maximal concentration of peptide (IC_{50}) required to inhibit the binding of the high affinity peptide SIINFEK- $T_{AMRA}L$. (G) Calculated free energy change (potential of mean force, PMF) obtained from umbrella sampling simulations along the distance between the $P\omega$ alpha carbon and the bottom of the F pocket. Free energy changes were extracted from simulations of complexes with peptides as indicated. (H) BFA decay experiment performed with RMA-S cells. H-2 K^b surface levels were determined at each time point with MA b Y3 and flow cytometry. Averages \pm SEM ($n = 3$) are normalized to initial mean fluorescence intensity (MFI).

(DOCX)

S2 Fig. Number of clusters as a function of cumulative simulation time. (A) complexes with SIINFEKL-derived peptides (B) complexes with FAPGNYPAL-derived peptides.

(DOCX)

S3 Fig. Representative snapshots of the start and end of the reaction coordinates used for the calculations of the free energy change (potential of mean force, PMF) obtained from umbrella sampling simulations along the distance between the $P\omega$ alpha carbone and the bottom of the F pocket.

(DOCX)

S4 Fig. Thermal denaturation of low-affinity peptide complexes is dependent of the concentration of free peptide. TDTF experiments were performed with the H-2 K^b -h β_2m -peptide complex in the presence of different peptide concentration. The T_m values of low-affinity peptide complexes increase with the free peptide concentration, but the relative difference in the T_m values between the C-terminal and N-terminal truncation remains.

(DOCX)

S1 Protocol. Detailed Protocols.

(DOCX)

S1 Table. Experimental and calculated binding free energy (kcal/mol) using MM-PBSA and TDTF methods for H-2 K^b /peptide complexes. The error is calculated as standard deviations over the defined clusters.

(DOCX)

S2 Table. Thermal denaturation measured by tryptophan fluorescence (TDTF) shows the T_m of K^b/β_2m empty or in complex with peptide, as indicated. The error is calculated as standard deviation.

(DOCX)

Acknowledgments

We would like to thank Zeynep Hein, Malgorzata Garstka, and Susanne Fritzsche for initial experiments; Uschi Wellbrock, Katja Ostermeir, Fabian Zeller, Florian Kandzia, and Giuseppe La Rosa for excellent technical assistance and scientific discussion. Our work was supported by Jacobs University and by the DAAD (German Academic Exchange Service) (to E.T.A.).

Author Contributions

Conceived and designed the experiments: ETA MZ SS. Performed the experiments: EA SKS VRR FTI. Analyzed the data: ETA SKS VRR FTI. Contributed reagents/materials/analysis tools: ETA MZ SS. Wrote the paper: ETA SS.

References

1. Yewdell JW (2006) Confronting complexity: real-world immunodominance in antiviral CD8+ T cell responses. *Immunity* 25: 533–543. PMID: [17046682](#)
2. Yaneva R, Schneeweiss C, Zacharias M, Springer S (2010) Peptide binding to MHC class I and II proteins: new avenues from new methods. *Mol Immunol* 47: 649–657. doi: [10.1016/j.molimm.2009.10.008](#) PMID: [19910050](#)
3. Reichen C, Hansen S, Pluckthun A (2014) Modular peptide binding: from a comparison of natural binders to designed armadillo repeat proteins. *J Struct Biol* 185: 147–162. doi: [10.1016/j.jsb.2013.07.012](#) PMID: [23916513](#)
4. Madden DR (1995) The three-dimensional structure of peptide-MHC complexes. *Annu Rev Immunol* 13: 587–622. PMID: [7612235](#)
5. Garrett TP, Saper MA, Bjorkman PJ, Strominger JL, Wiley DC (1989) Specificity pockets for the side chains of peptide antigens in HLA-Aw68. *Nature* 342: 692–696. PMID: [2594067](#)
6. Sieker F, Straatsma TP, Springer S, Zacharias M (2008) Differential tapasin dependence of MHC class I molecules correlates with conformational changes upon peptide dissociation: a molecular dynamics simulation study. *Mol Immunol* 45: 3714–3722. doi: [10.1016/j.molimm.2008.06.009](#) PMID: [18639935](#)
7. Persson K, Schneider G (2000) Three-dimensional structures of MHC class I-peptide complexes: implications for peptide recognition. *Arch Immunol Ther Exp (Warsz)* 48: 135–142.
8. Barber LD, Parham P (1993) Peptide binding to major histocompatibility complex molecules. *Annu Rev Cell Biol* 9: 163–206. PMID: [7506551](#)
9. Young AC, Nathenson SG, Sacchettini JC (1995) Structural studies of class I major histocompatibility complex proteins: insights into antigen presentation. *FASEB J* 9: 26–36. PMID: [7821756](#)
10. Rao X, Costa AI, van Baarle D, Kesmir C (2009) A comparative study of HLA binding affinity and ligand diversity: implications for generating immunodominant CD8+ T cell responses. *J Immunol* 182: 1526–1532. PMID: [19155500](#)
11. Fremont DH, Stura EA, Matsumura M, Peterson PA, Wilson IA (1995) Crystal structure of an H-2Kb-ovalbumin peptide complex reveals the interplay of primary and secondary anchor positions in the major histocompatibility complex binding groove. *Proc Natl Acad Sci U S A* 92: 2479–2483. PMID: [7708669](#)
12. Bouvier M, Wiley DC (1994) Importance of peptide amino and carboxyl termini to the stability of MHC class I molecules. *Science* 265: 398–402. PMID: [8023162](#)
13. Christensen O, Lupu A, Schmidt S, Condomines M, Belle S, et al. (2009) Melan-A/MART1 analog peptide triggers anti-myeloma T-cells through crossreactivity with HM1.24. *J Immunother* 32: 613–621. doi: [10.1097/CJI.0b013e3181a95198](#) PMID: [19483648](#)
14. Hamdahl M, Rasmussen M, Roder G, Pedersen ID, Sorensen M, et al. (2012) Peptide-MHC class I stability is a better predictor than peptide affinity of CTL immunogenicity. *European Journal of Immunology* 42: 1405–1416. doi: [10.1002/eji.201141774](#) PMID: [22678897](#)
15. Lewis JW, Neisig A, Neefjes J, Elliott T (1996) Point mutations in the alpha 2 domain of HLA-A2.1 define a functionally relevant interaction with TAP. *Curr Biol* 6: 873–883. PMID: [8805302](#)
16. Zernich D, Purcell AW, Macdonald WA, Kjer-Nielsen L, Ely LK, et al. (2004) Natural HLA class I polymorphism controls the pathway of antigen presentation and susceptibility to viral evasion. *J Exp Med* 200: 13–24. PMID: [15226359](#)
17. Simone LC, Georges CJ, Simone PD, Wang X, Solheim JC (2012) Productive association between MHC class I and tapasin requires the tapasin transmembrane/cytosolic region and the tapasin C-terminal Ig-like domain. *Mol Immunol* 49: 628–639. doi: [10.1016/j.molimm.2011.11.002](#) PMID: [22169163](#)
18. Dong G, Wearsch PA, Peaper DR, Cresswell P, Reinisch KM (2009) Insights into MHC class I peptide loading from the structure of the tapasin-ERp57 thiol oxidoreductase heterodimer. *Immunity* 30: 21–32. doi: [10.1016/j.immuni.2008.10.018](#) PMID: [19119025](#)
19. Kurimoto E, Kuroki K, Yamaguchi Y, Yagi-Utsumi M, Igaki T, et al. (2013) Structural and functional mosaic nature of MHC class I molecules in their peptide-free form. *Mol Immunol* 55: 393–399. doi: [10.1016/j.molimm.2013.03.014](#) PMID: [23578712](#)

20. Bouvier M, Wiley DC (1998) Structural characterization of a soluble and partially folded class I major histocompatibility heavy chain/beta 2m heterodimer. *Nat Struct Biol* 5: 377–384. PMID: [9587000](#)
21. Kienast A, Preuss M, Winkler M, Dick TP (2007) Redox regulation of peptide receptivity of major histocompatibility complex class I molecules by ERp57 and tapasin. *Nat Immunol* 8: 864–872. PMID: [17603488](#)
22. Springer S, Doring K, Skipper JC, Townsend AR, Cerundolo V (1998) Fast association rates suggest a conformational change in the MHC class I molecule H-2Db upon peptide binding. *Biochemistry* 37: 3001–3012. PMID: [9485452](#)
23. Zacharias M, Springer S (2004) Conformational flexibility of the MHC class I alpha 1-alpha 2 domain in peptide bound and free states: a molecular dynamics simulation study. *Biophys J* 87: 2203–2214. PMID: [15454423](#)
24. Narzi D, Becker CM, Fiorillo MT, Uchanska-Ziegler B, Ziegler A, et al. (2012) Dynamical characterization of two differentially disease associated MHC class I proteins in complex with viral and self-peptides. *J Mol Biol* 415: 429–442. doi: [10.1016/j.jmb.2011.11.021](#) PMID: [22119720](#)
25. Bailey A, van Hateren A, Elliott T, Werner JM (2014) Two polymorphisms facilitate differences in plasticity between two chicken major histocompatibility complex class I proteins. *PLoS One* 9: e89657. doi: [10.1371/journal.pone.0089657](#) PMID: [24586943](#)
26. Fabian H, Huser H, Narzi D, Misselwitz R, Loll B, et al. (2008) HLA-B27 subtypes differentially associated with disease exhibit conformational differences in solution. *J Mol Biol* 376: 798–810. doi: [10.1016/j.jmb.2007.12.009](#) PMID: [18178223](#)
27. Elliott T (1997) How does TAP associate with MHC class I molecules? *Immunology Today* 18: 375–379. PMID: [9267079](#)
28. Wright CA, Kozik P, Zacharias M, Springer S (2004) Tapasin and other chaperones: models of the MHC class I loading complex. *Biological Chemistry* 385: 763–778. PMID: [15493870](#)
29. Rammensee H, Bachmann J, Emmerich NP, Bachor OA, Stevanovic S (1999) SYFPEITHI: database for MHC ligands and peptide motifs. *Immunogenetics* 50: 213–219. PMID: [10602881](#)
30. Vita R, Zarebski L, Greenbaum JA, Emami H, Hoof I, et al. (2010) The immune epitope database 2.0. *Nucleic Acids Res* 38: D854–862. doi: [10.1093/nar/gkp1004](#) PMID: [19906713](#)
31. Glithero A, Tormo J, Doering K, Kojima M, Jones EY, et al. (2006) The crystal structure of H-2D(b) complexed with a partial peptide epitope suggests a major histocompatibility complex class I assembly intermediate. *J Biol Chem* 281: 12699–12704. PMID: [16478731](#)
32. Saini SK, Ostermeier K, Ramnarayan VR, Schuster H, Zacharias M, et al. (2013) Dipeptides promote folding and peptide binding of MHC class I molecules. *Proc Natl Acad Sci U S A* 110: 15383–15388. doi: [10.1073/pnas.1308672110](#) PMID: [24003162](#)
33. Mage MG, Dolan MA, Wang R, Boyd LF, Revilla MJ, et al. (2012) The peptide-receptive transition state of MHC class I molecules: insight from structure and molecular dynamics. *J Immunol* 189: 1391–1399. doi: [10.4049/jimmunol.1200831](#) PMID: [22753930](#)
34. Hein Z, Uchtenhagen H, Abualrous ET, Saini SK, Janssen L, et al. (2014) Peptide-independent stabilization of MHC class I molecules breaches cellular quality control. *J Cell Sci* 127: 2885–2897. doi: [10.1242/jcs.145334](#) PMID: [24806963](#)
35. Sieker F, Springer S, Zacharias M (2007) Comparative molecular dynamics analysis of tapasin-dependent and-independent MHC class I alleles. *Protein Sci* 16: 299–308. PMID: [17242432](#)
36. Saini SK, Abualrous ET, Tigan AS, Covella K, Wellbrock U, et al. (2013) Not all empty MHC class I molecules are molten globules: tryptophan fluorescence reveals a two-step mechanism of thermal denaturation. *Mol Immunol* 54: 386–396. doi: [10.1016/j.molimm.2013.01.004](#) PMID: [23391462](#)
37. Ljunggren HG, Stam NJ, Ohlen C, Neeffjes JJ, Hoglund P, et al. (1990) Empty MHC class I molecules come out in the cold. *Nature* 346: 476–480. PMID: [2198471](#)
38. Sieker F, May A, Zacharias M (2009) Predicting affinity and specificity of antigenic peptide binding to major histocompatibility class I molecules. *Curr Protein Pept Sci* 10: 286–296. PMID: [19519456](#)
39. Garstka MA, Fritzsche S, Lenart I, Hein Z, Jankevicius G, et al. (2011) Tapasin dependence of major histocompatibility complex class I molecules correlates with their conformational flexibility. *FASEB J* 25: 3989–3998. doi: [10.1096/fj.11-190249](#) PMID: [21836024](#)
40. Kuhn B, Kollman PA (2000) Binding of a diverse set of ligands to avidin and streptavidin: an accurate quantitative prediction of their relative affinities by a combination of molecular mechanics and continuum solvent models. *J Med Chem* 43: 3786–3791. PMID: [11020294](#)
41. Wang W, Kollman PA (2000) Free energy calculations on dimer stability of the HIV protease using molecular dynamics and a continuum solvent model. *J Mol Biol* 303: 567–582. PMID: [11054292](#)

42. Donini OA, Kollman PA (2000) Calculation and prediction of binding free energies for the matrix metalloproteinases. *J Med Chem* 43: 4180–4188. PMID: [11063614](#)
43. Pearlman DA (2005) Evaluating the molecular mechanics Poisson-Boltzmann surface area free energy method using a congeneric series of ligands to p38 MAP kinase. *Journal of Medicinal Chemistry* 48: 7796–7807. PMID: [16302819](#)
44. Kuhn B, Gerber P, Schulz-Gasch T, Stahl M (2005) Validation and use of the MM-PBSA approach for drug discovery. *Journal of Medicinal Chemistry* 48: 4040–4048. PMID: [15943477](#)
45. Miyamoto S, Kollman PA (1993) Absolute and Relative Binding Free-Energy Calculations of the Interaction of Biotin and Its Analogs with Streptavidin Using Molecular-Dynamics Free-Energy Perturbation Approaches. *Proteins-Structure Function and Genetics* 16: 226–245.
46. Sun HY, Li YY, Tian S, Xu L, Hou TJ (2014) Assessing the performance of MM/PBSA and MM/GBSA methods. 4. Accuracies of MM/PBSA and MM/GBSA methodologies evaluated by various simulation protocols using PDBbind data set. *Physical Chemistry Chemical Physics* 16: 16719–16729. doi: [10.1039/c4cp01388c](#) PMID: [24999761](#)
47. Page CS, Bates PA (2006) Can MM-PBSA calculations predict the specificities of protein kinase inhibitors? *Journal of Computational Chemistry* 27: 1990–2007. PMID: [17036304](#)
48. Hou TJ, Wang JM, Li YY, Wang W (2011) Assessing the Performance of the MM/PBSA and MM/GBSA Methods. 1. The Accuracy of Binding Free Energy Calculations Based on Molecular Dynamics Simulations. *Journal of Chemical Information and Modeling* 51: 69–82. doi: [10.1021/ci100275a](#) PMID: [21117705](#)
49. Lakowicz JR (2006) *Principles of Fluorescence Spectroscopy*. New York/Heidelberg: Springer.
50. Eftink MR (1994) The Use of Fluorescence Methods to Monitor Unfolding Transitions in Proteins. *Biophysical Journal* 66: 482–501. PMID: [8161701](#)
51. Saini SK, Abualrous ET, Tigan AS, Covella K, Wellbrock U, et al. (2013) Not all empty MHC class I molecules are molten globules: Tryptophan fluorescence reveals a two-step mechanism of thermal denaturation. *Molecular Immunology* 54: 386–396. doi: [10.1016/j.molimm.2013.01.004](#) PMID: [23391462](#)
52. Rupp B, Gunther S, Makhmoo T, Schlundt A, Dickhaut K, et al. (2011) Characterization of structural features controlling the receptiveness of empty class II MHC molecules. *PLoS One* 6: e18662. doi: [10.1371/journal.pone.0018662](#) PMID: [21533180](#)
53. Kumar A, Cocco E, Atzori L, Marrosu MG, Pieroni E (2013) Structural and dynamical insights on HLA-DR2 complexes that confer susceptibility to multiple sclerosis in Sardinia: a molecular dynamics simulation study. *PLoS One* 8: e59711. doi: [10.1371/journal.pone.0059711](#) PMID: [23555757](#)
54. Yaneva R, Springer S, Zacharias M (2009) Flexibility of the MHC class II peptide binding cleft in the bound, partially filled, and empty states: a molecular dynamics simulation study. *Biopolymers* 91: 14–27. doi: [10.1002/bip.21078](#) PMID: [18767126](#)
55. Wright CA, Kozik P, Zacharias M, Springer S (2004) Tapasin and other chaperones: models of the MHC class I loading complex. *Biol Chem* 385: 763–778. PMID: [15493870](#)
56. Dedier S, Reinelt S, Rion S, Folkers G, Rognan D (2001) Use of fluorescence polarization to monitor MHC-peptide interactions in solution. *J Immunol Methods* 255: 57–66. PMID: [11470286](#)
57. Townsend A, Ohlen C, Foster L, Bastin J, Ljunggren HG, et al. (1989) A mutant cell in which association of class I heavy and light chains is induced by viral peptides. *Cold Spring Harb Symp Quant Biol* 54 Pt 1: 299–308.
58. Ljunggren HG, Karre K (1985) Host resistance directed selectively against H-2-deficient lymphoma variants. Analysis of the mechanism. *J Exp Med* 162: 1745–1759. PMID: [3877776](#)
59. Falk K, Rotzschke O, Stevanovic S, Jung G, Rammensee HG (1991) Allele-specific motifs revealed by sequencing of self-peptides eluted from MHC molecules. *Nature* 351: 290–296. PMID: [1709722](#)
60. Koch CP, Perna AM, Pillong M, Todoroff NK, Wrede P, et al. (2013) Scrutinizing MHC-I binding peptides and their limits of variation. *PLoS Comput Biol* 9: e1003088. doi: [10.1371/journal.pcbi.1003088](#) PMID: [23754940](#)
61. Natarajan K, Li H, Mariuzza RA, Margulies DH (1999) MHC class I molecules, structure and function. *Rev Immunogenet* 1: 32–46. PMID: [11256571](#)
62. Johansen TE, McCullough K, Catipovic B, Su XM, Amzel M, et al. (1997) Peptide binding to MHC class I is determined by individual pockets in the binding groove. *Scand J Immunol* 46: 137–146. PMID: [9583994](#)
63. Reboul CF, Meyer GR, Porebski BT, Borg NA, Buckle AM (2012) Epitope flexibility and dynamic footprint revealed by molecular dynamics of a pMHC-TCR complex. *PLoS Comput Biol* 8: e1002404. doi: [10.1371/journal.pcbi.1002404](#) PMID: [22412359](#)

64. Gao B, Adhikari R, Howarth M, Nakamura K, Gold MC, et al. (2002) Assembly and antigen-presenting function of MHC class I molecules in cells lacking the ER chaperone calreticulin. *Immunity* 16: 99–109. PMID: [11825569](#)
65. Chefalo PJ, Harding CV (2001) Processing of exogenous antigens for presentation by class I MHC molecules involves post-Golgi peptide exchange influenced by peptide-MHC complex stability and acidic pH. *J Immunol* 167: 1274–1282. PMID: [11466343](#)
66. Chen L, Jondal M (2004) Endolysosomal processing of exogenous antigen into major histocompatibility complex class I-binding peptides. *Scandinavian Journal of Immunology* 59: 545–552. PMID: [15182249](#)
67. Yanaka S, Ueno T, Shi Y, Qi J, Gao GF, et al. (2014) Peptide-dependent Conformational Fluctuation Determines the Stability of the Human Leukocyte Antigen Class I Complex. *J Biol Chem* 289: 24680–24690. doi: [10.1074/jbc.M114.566174](#) PMID: [25028510](#)
68. Sharp K (2001) Entropy-enthalpy compensation: fact or artifact? *Protein Sci* 10: 661–667. PMID: [11344335](#)
69. Fenley AT, Muddana HS, Gilson MK (2012) Entropy-enthalpy transduction caused by conformational shifts can obscure the forces driving protein-ligand binding. *Proc Natl Acad Sci U S A* 109: 20006–20011. doi: [10.1073/pnas.1213180109](#) PMID: [23150595](#)
70. Dunitz JD (1995) Win Some, Lose Some—Enthalpy-Entropy Compensation in Weak Intermolecular Interactions. *Chemistry & Biology* 2: 709–712.
71. Stites WE (1997) Protein-protein interactions: Interface structure, binding thermodynamics, and mutational analysis. *Chemical Reviews* 97: 1233–1250. PMID: [11851449](#)
72. Reiser JB, Darnault C, Gregoire C, Mosser T, Mazza G, et al. (2003) CDR3 loop flexibility contributes to the degeneracy of TCR recognition. *Nature Immunology* 4: 241–247. PMID: [12563259](#)
73. Garstka M, Borchert B, Al-Balushi M, Praveen PV, Kuhl N, et al. (2007) Peptide-receptive major histocompatibility complex class I molecules cycle between endoplasmic reticulum and cis-Golgi in wild-type lymphocytes. *J Biol Chem* 282: 30680–30690. PMID: [17656363](#)
74. Chen M, Bouvier M (2007) Analysis of interactions in a tapasin/class I complex provides a mechanism for peptide selection. *EMBO J* 26: 1681–1690. PMID: [17332746](#)
75. Smock RG, Rivoire O, Russ WP, Swain JF, Leibler S, et al. (2010) An interdomain sector mediating allostery in Hsp70 molecular chaperones. *Mol Syst Biol* 6: 414. doi: [10.1038/msb.2010.65](#) PMID: [20865007](#)